Chapter 6
Nonlinear Optical Properties of Nanomaterials

Pranitha Sankar and Reji Philip

6.1 Introduction

Nonlinear optics (NLO) involves the study of the interaction of intense light fields with matter. After the invention of the laser in 1960, Franken and colleagues [1] observed second harmonic generation (SHG) of ruby laser beam in a quartz crystal, which was followed by similar studies in various materials. Thereafter, Bloembergen and colleagues formulated a general theoretical framework for three- and four-wave mixing at optical frequencies [2]. The quantum mechanical calculation of complex nonlinear susceptibilities, based on the evolution of the density matrix (see for example, [3, 4]), was subsequently applied to optical problems. In 1965 Rentzepis and Pao reported the first observation of SHG in an organic material (benzpyrene) [5].

The field of NLO grew substantially over the years, facilitating a deeper understanding of light-matter interaction and providing solutions for several technological problems. Efficient nonlinear optical interactions have become essential for many applications in advanced photonics. However, they typically require intense laser sources, different wavelengths and interaction lengths, in order to utilize nonlinear optics for novel nanophotonic architectures in integrated optics and metasurface devices. Obtaining materials with stronger nonlinear properties is an important step towards applications. For example, certain essential devices in the telecom industry such as switches, routers, and wavelength converters can be realized using optical nonlinearity. While second order nonlinearities mostly involve optical frequency

P. Sankar
Institut Für Quantenoptik, Leibniz Universität Hannover, 30167 Hannover, Germany

R. Philip (✉)
Light and Matter Physics Group, Raman Research Institute, C. V. Raman Avenue, Sadashivanagar, Bangalore 560080, India
e-mail: reji@rri.res.in

S. S. Nair and R. Philip, *Nanomaterials for Luminescent Devices, Sensors, and Bio-imaging Applications*, Progress in Optical Science and Photonics 16,
https://doi.org/10.1007/978-981-16-5367-4_6

conversion, third order phenomena include nonlinear phase modulation, nonlinear absorption and nonlinear scattering of light. Nanoparticles and nanocomposites have become important materials for nonlinear optics in recent years because of their interesting surface effects and properties such as quantum confinement, plasmon oscillations etc., which are absent in the corresponding bulk materials. The remarkable NLO properties displayed by nanomaterials have motivated the design and fabrication of nanoscale photonic and optoelectronic devices [6]. Several practical optical devices using 2-D layered materials, such as optical modulators, optical polarizers, optical switchers, and even all-optical devices, are expected to be developed in the near future [7].

Carbon-based nanomaterials such as 0D fullerenes, 1D carbon nanotubes (CNT) and 2D graphenes [8] have become essential materials for nanotechnology, and their spectacular mechanical, electrical and thermal properties, in addition to their distinctive NLO properties, have generated substantial research interest from both academic and industrial aspects [9–11]. Metamaterials are another class of engineered materials made from meta-atom building blocks organized into arrays of subwavelength metal and/or dielectric components. Strong light-matter interaction in metamaterials results in novel linear and nonlinear optical (NLO) properties [12], making them attractive for applications in sensing, terahertz imaging, and optical fiber manufacture. Recently, it has been established that materials with a vanishingly small permittivity can enable efficient nonlinear optical phenomena [13]. These materials are commonly known as epsilon-near-zero (ENZ) materials, and they exhibit unprecedented ultrafast nonlinear efficiencies within sub-wavelength propagation lengths with low optical losses and high nonlinear enhancements [14].

In this chapter we will outline the physical origins of optical nonlinearity in material media, and discuss the nonlinear optical properties reported for advanced nanomaterials in recent years. Experimental techniques will be explained and results obtained in different nanomaterials will be overviewed.

6.2 The Nonlinear Susceptibility

A steady electric field **E** applied to a dielectric medium generates an ensemble of induced dipoles. The net average dipole moment per unit volume (electric polarization) is given by

$$\mathbf{P} = N\langle\mu\rangle \tag{6.1}$$

where N is the number of microscopic dipoles per unit volume, and $\langle\mu\rangle$ is the ensemble averaged induced dipole moment. **P** can also be written in the form

$$\mathbf{P_i} = \varepsilon_0 \chi_{ij}^{(1)} \mathbf{E_j} \tag{6.2}$$

where ε_0 is the vacuum dielectric constant, $\chi_{ij}^{(1)}$ w is the linear susceptibility, and $\mathbf{E_j}$ is the amplitude of the electric field vector. $\chi_{ij}^{(1)}$ is a second rank tensor since it relates the two vector quantities $\mathbf{P_i}$ and $\mathbf{E_j}$. Now, it is possible to consider the electric field of electromagnetic radiation in the place of a steady electric field, in which case $\mathbf{E_j}$ and $\mathbf{P_i}$ become rapidly oscillating vector fields. The linear optical properties of the medium, viz. the refractive index (n_0) and absorption coefficient (α_0), are then derived from $\chi_{ij}^{(1)}$.

To interpret the observed effects of second order and third order nonlinearities in different materials, it is necessary to speculate that under the action of an intense laser, the dielectric strength of the medium is no longer linearly related to the amplitude of the incident light field. If the intensity of the exciting electromagnetic radiation is sufficiently strong, the dipole oscillations become anharmonic. The polarization will have a nonlinear dependence on the electric field in this case [4], which can be written as a power series expansion

$$\mathbf{P_i} = \varepsilon_0\left\{\chi_{ij}^{(1)} \cdot \mathbf{E_j} + \chi_{ijk}^{(2)} \cdot \mathbf{E_j E_k} + \chi_{ijkl}^{(3)} \cdot \mathbf{E_j E_k E_l} + \cdots\right\} \tag{6.3}$$

where $\chi_{ijk}^{(2)}$ and $\chi_{ijkl}^{(3)}$ are the second order and third order nonlinear optical susceptibilities respectively. In general, the dipole response to an applied field can always be considered as anharmonic, and therefore Eq. (6.3) becomes the generalized equation for the response of a medium to electromagnetic radiation.

The magnitude of the optical nonlinearity will depend on the applied light field intensity and the nonlinear susceptibility coefficients. $\chi^{(2)}$ leads to second order nonlinearities and $\chi^{(3)}$ leads to third order nonlinearities in the medium. Media with inversion symmetry do not exhibit nonlinearities of even order, while those without a symmetry axis display nonlinearity of both even and odd orders. Therefore, while the lowest nonlinearity in anisotropic crystals is of the second order, that in isotropic media like liquids, gases and amorphous solids (e.g.: glass) is of the third order.

While second order nonlinearities in crystals mostly lead to frequency conversion phenomena such as harmonic generation and parametric mixing, the third order nonlinear susceptibility $\chi^{(3)}$ contributes to nonlinear refraction, nonlinear absorption, and nonlinear scattering (stimulated Raman and stimulated Brillouin scattering) effects.

6.3 Nonlinear Refraction and Absorption

Nonlinear refraction occurs when there is a change in the refractive index of a medium due to the presence of external fields. A number of physical effects such as optical Kerr effect, thermal lensing, electrostriction and population redistribution can contribute to nonlinear index of refraction. It may be noted that some of these like thermal lensing are resonant phenomena and the calculation of the corresponding susceptibilities

requires a treatment which is different from the perturbative approach adopted in Eq. 6.3.

Considering the optical Kerr effect, the real and imaginary parts of the corresponding degenerate nonlinear susceptibility, $\chi^{(3)}$ (ω; ω, $-\omega$, ω) are related to self-focusing and two-photon absorption. These are given by [15]

$$\text{Re}\,\chi^{(3)} = (4/3)n_0^2 n_2 \varepsilon_0 c \tag{6.4}$$

and

$$\text{Im}\,\chi^{(3)} = (\lambda/3\pi)n_0^2 \alpha_2 \varepsilon_0 c \tag{6.5}$$

where λ is the light wavelength in meters, c is the light velocity in ms^{-1}, α_2 is the two-photon absorption coefficient in mW^{-1}, and n_2 is the nonlinear refractive index in m^2W^{-1}. The net refractive index of the medium is given by $n = n_0 + n_2 I$, where I is the light intensity in Wm^{-2}. I is related to the optical field E through the relation

$$I = 2n_0(\varepsilon_0/\mu_0)^{1/2}|E|^2 = (2n_0/Z_0)|E|^2 \tag{6.6}$$

where $\varepsilon_0 = 8.85 \times 10^{-12}\,F\,m^{-1}$ is the permittivity, $\mu_0 = 4\pi \times 10^{-7}$ H/m is the permeability, and $Z_0 = 377\ \Omega$ is the characteristic impedance, of free space. Depending on whether n_2 is positive or negative, the modification in the refractive index will give rise to self-focusing or defocusing effects. Similarly, the net absorption coefficient is given by $\alpha = \alpha_0 + \alpha_2 I$, so that a modified Beer-Lambert law can be written in the form

$$I = I_0 e^{-(\alpha_0 + \alpha_2 I)z} \tag{6.7}$$

where z is the direction of propagation. A positive α_2 will lead to enhanced absorption while a negative α_2 will lead to enhanced transmission.

Nonlinear refraction has potential applications in optical switching, optical limiting, passive laser mode-locking, and waveguide switches and modulators. At low light levels the absorption coefficient of a medium does not depend on of the input light intensity. At high intensities, however, several phenomena can take place that can modify this behavior. For instance, absorption can get saturated as the excited state population increases. Alternatively, the excited states can absorb photons, sometimes even stronger than the ground state. Similarly, photo-generated free carriers in semiconductors may absorb more photons. Another possibility is that of two or more photons getting absorbed in a single event. All these phenomena will change the transmittance of the medium at high intensities, causing a deviation from the Beer-Lambert law. This change in transmittance of a material with input light intensity or fluence is generally known as nonlinear absorption. A few of these

processes are saturable absorption, excited state absorption, multi-photon absorption and free-carrier absorption.

6.4 Measurement of Second Order Nonlinearities

Second-order nonlinear optical (NLO) materials have attracted much attention primarily because of their excellent ability for wavelength conversion. Experimental methods in second order NLO are usually devised to measure either the nonlinear coefficient d_{eff} or the first order hyperpolarizability β. Two absolute measurement methods often used are the phase-matched method and parametric fluorescence method respectively. Maker fringe method [16] and Kurtz powder method [17] are the relative measurement techniques employed for characterizing the medium with respect to a standard reference material. These techniques are useful when the sample is in single crystal form. For thin films reflectance measurements can be done, and the poling technique [15] is found to be useful for polymer thin films.

While developing new materials for NLO it may often be convenient to characterize individual molecules initially, before proceeding to study the bulk material. This is particularly true for organic media since bulk properties are largely determined by the individual molecular units. Relative methods for characterizing molecular parameters include Electric field induced second harmonic generation (EFISH) [18] which is useful in the case of neutral, dipolar molecules, and Hyper-Rayleigh Scattering (HRS) [19] for non-dipolar or charged molecules. Various theoretical approaches have been developed for the calculation of the molecular hyperpolarizability [20]. Even though the above methods are most useful approaches for chemists to understand structure–hyperpolarizability relationships, and for designing new, highly efficient second-order NLO molecular materials.

6.5 Measurement of Third Order Nonlinearities

Experimental methods for third order nonlinearity determination include Third harmonic generation, degenerate four wave mixing, Z-scan, optical Kerr effect, and two-photon fluorescence. Of these, the Z-scan is the simplest technique to implement. Within a short period of its invention the Z-scan has become a major method for measuring the nonlinear refraction and absorption coefficients in materials.

Z-scan: The nonlinear absorption coefficient and nonlinear refractive index of a material can be measured using the open aperture and closed aperture Z-scan techniques respectively [21]. In the open aperture configuration, a laser beam having a Gaussian spatial distribution is initially focused by a lens. The beam direction is taken as the z axis, and the beam focus is taken as $z = 0$. The sample to be measured is then translated in short steps from a negative z position to a positive z position through the focal point. The sample transmission corresponding to each z position is

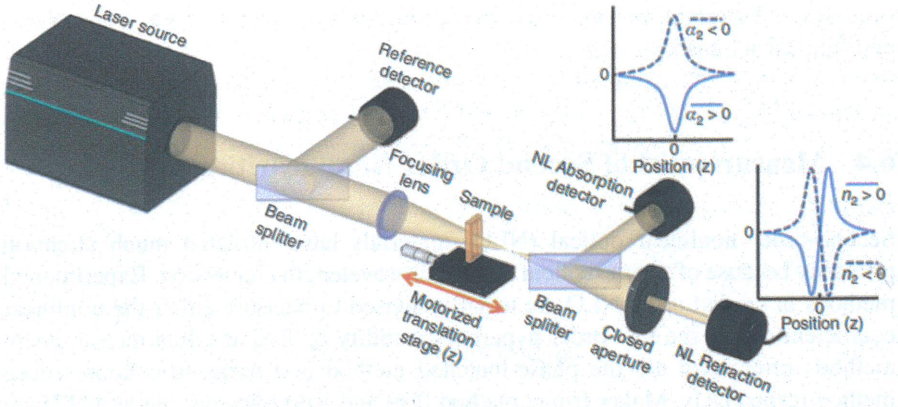

Fig. 6.1 Schematic of a simultaneous open aperture and closed aperture Z-scan experiment. The NL absorption detector measures open aperture signal while the NL refraction detector measures closed aperture signal, as a function of sample position (from Ref. [12])

measured using a detector placed after the sample. A graph in which the measured transmission (usually normalized to the linear transmission value) is plotted against z is known as the Z-scan curve. In the closed aperture Z-scan a small aperture is placed in front of the detector, which makes the measurement sensitive to beam size variations due to nonlinear refraction. The Z-scan experimental set up is shown in Fig. 6.1.

Open aperture Z-scan: In open aperture Z-scan no aperture will be kept in front of the detector, and therefore, the detector will measure all of the light transmitted by the sample. When the sample is at the focal point its transmission will be either a maximum or minimum, depending on the sign of the dominant nonlinear mechanism. For reverse saturable absorption the transmittance will be a minimum, and for saturable absorption it will be a maximum. In general, an open-aperture Z-scan trace will be symmetric with respect to the focus ($z = 0$). The normalized transmittance of a laser pulse through a third order nonlinear medium is given by [21]

$$T(z) = \left[\frac{1}{\pi^{\frac{1}{2}} q(z)}\right] \int_{-\infty}^{+\infty} \ln\left[1 + q(z)\exp\left(-\tau^2\right)\right] d\tau \tag{6.8}$$

with $q(z) = \alpha_2 I_0 L_{eff}/[1 + (z/z_0)^2]$, where I_0 is the peak intensity at the focal point. α_2 denotes the nonlinear absorption coefficient. For a medium that is transparent at the excitation wavelength, α_2 will be the two-photon absorption coefficient. The magnitude and sign of α_2 can be determined by numerically fitting the open aperture Z-scan curve to Eq. 6.8. Expressions for Z-scan transmittance under multiphoton excitation conditions are available in literature [22, 23].

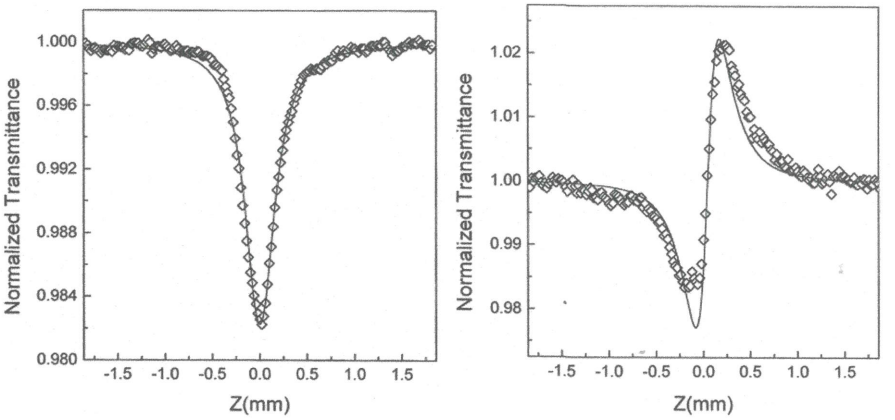

Fig. 6.2 Open aperture and closed aperture Z-scan curves measured in Ag nanorods dispersed in borosilicate glass, using 800 nm, 240 fs laser pulses at an intensity of 8.8×10^9 W/cm^2. Numerical fits (solid curves) to the experimental data (squares) reveal a third order nonlinearity, giving an α_2 value of 1.73×10^{-9} cm W^{-1} and n_2 value of 2.0×10^4 cm^2/GW (From Ref. [89])

A typical open-aperture Z-scan curve, measured in Ag nanorods dispersed in borosilicate glass, is shown in Fig. 6.2. The figure shows a "valley" which is typical for samples showing two-photon absorption or excited state absorption. In this case, the presence of the strong surface plasmon resonance (SPR) band around 400 nm facilitates strong two-photon absorption when the nanorods are excited at 800 nm.

Closed aperture Z-scan: The closed aperture Z-scan measurement is based on the self-focusing or self-defocusing of a spatially Gaussian optical beam occurring in a thin nonlinear medium. A plot of normalized transmittance versus sample position in this configuration will give information regarding the real part of the nonlinearity (nonlinear refractive index). As mentioned earlier, the net refractive index of a medium with a Kerr nonlinearity can be written as $n = n_0 + n_2 I$, where n_0 is the linear refractive index, n_2 is the nonlinear refractive index coefficient, and I is the time averaged intensity of the optical field. Now consider a laser beam with a Gaussian beam cross section, given by $I = I_0 \exp(-2r^2/\omega^2)$, where ω is the beam radius and r is the radial co-ordinate. The intensity of the beam will be a maximum at the center, and will drop along the radial direction. Therefore, when a Gaussian laser beam passes through a nonlinear medium its refractive index will be modified in such a way that maximum change occurs at the beam center. This results in a phase modulation of the wavefront such that the beam gets focused if n_2 is positive, and de-focused if n_2 is negative. Thus the medium will behave as a nonlinear lens, the focal length of which is intensity-dependent, and hence depends on the sample position z. Therefore, if a small aperture is placed in front of the detector, then the aperture transmittance will become a function of z. Such focusing/defocusing is usually small in magnitude, and a sufficiently high intensity (I), as from a pre-focused beam, is normally required to get a measurable effect.

A typical closed aperture Z-scan measured in Ag nanorods at the excitation wavelength of 800 nm is shown in Fig. 6.2. The figure shows a "valley and peak" structure. This symmetric "valley-peak" structure is typical for a sample that shows self-focusing (a "peak-valley" structure will appear for a self-defocusing sample). The difference in normalized transmittance between the peak and the valley, ΔT_{p-v}, is a measure of the nonlinear refractive index of the medium. From numerical fits to theory, the nonlinear refractive index of the Ag nanorods is calculated to be $n_2 = 2.0 \times 10^4$ cm^2/GW.

Considering a thin nonlinear medium (i.e., $l \ll z_R$ where l is the sample length and $z_R = \pi\omega_0^2/\lambda$ is the Rayleigh range of the focused beam in air, where ω_0 is the $1/e^2$ beam radius at focus and λ is the excitation wavelength), exhibiting the optical Kerr effect and having no nonlinear absorption, the nonlinear phase $\Delta\phi(z, t)$ impressed on the wave is given by

$$\Delta\phi(z, t) = \Delta\phi_0(t)/\left[1 + (z/z_R)^2\right] \tag{6.9}$$

When the sample is at the beam focus the phase distortion will be a maximum. If the on-axis phase shift is small (i.e., when $|\Delta\phi_0| < \pi$), then ΔT_{p-v} is approximately (within a precision of 3%) given by

$$\Delta T_{p-v} = 0.405(1 - S)^{0.25} < \Delta\phi_0 > \tag{6.10}$$

where S is the linear aperture transmittance given by $1 - \exp(-2r_a^2/\omega_a^2)$. Here r_a is the aperture radius and ω_a is the beam radius at the aperture. Knowing ΔT_{p-v} from the z-scan curve, $< \Delta\phi_0 >$ can be estimated using the above equation. The nonlinear refractive index coefficient can then be determined from the relation

$$\Delta T_{p-v} = 0.405(1 - S)^{0.25} < \Delta\phi_0 > \tag{6.11}$$

where E_i is the input energy, t_{FWHM} is the laser pulse width (full width at half maximum), and $L_{eff} = [1 - \exp(-\alpha_0 l)]/\alpha_0$.

If the on-axis phase shift is larger than π(like in the case of a strong thermal lens effect), then the above approximations have to be replaced by more precise expressions. Similarly, if the sample shows both nonlinear absorption and nonlinear refraction simultaneously, then the closed-aperture curve should be divided by the open aperture curve before carrying out the nonlinear refractive index calculations.

6.6 Enhancement of Optical Nonlinearities in Nanomaterials

In this section, we focus on the nonlinear optical response of plasmonic and carbon-based nanomaterials or their composites, which ideally possess NLO properties superior to those of the starting materials. These are classified into: '0' dimension materials like nanospheres and nanocrystals, '1' dimension materials like nanotubes and nanorods, and '2' dimension materials like nanofilms, nanofoils and nano surface layers. The usually encountered structures of nanomaterials can be classified into four different major groups, namely the Maxwell-Garnett geometry, Bruggeman geometry, layered structures, and fractal structures.

6.6.1 Maxwell-Garnett Geometry

In this geometry, the nanoparticle is dispersed randomly in a host material as shown in Fig. 6.3. According to this model, the particles are of uniform size and spherical shape. Optical properties of composite materials in this geometry can be understood in terms of local field effects. The concept of local fields [24] is important in standard discussions of the optical properties of homogenous nanomaterials. For example, in the presence of an oscillating electric field, metal nanospheres emit electric dipole radiation. Maxwell-Garnett theory replaces the spheres in the model by the equivalent point dipoles, i.e., their finite size is ignored. If **p** represents the average dipole moment of an inclusion and N represents the number of nanoparticles per unit volume, then the total polarization of the medium (normalized by the dielectric constant of the host) is given by,

$$\mathbf{P} = \mathrm{N}\mathbf{p} \tag{6.12}$$

The average dipole moment is given by,

$$\mathrm{p} = \mathrm{a}^3 \frac{\epsilon_\mathrm{i} - \epsilon_\mathrm{h}}{\epsilon_\mathrm{i} + 2\,\epsilon_\mathrm{h}} \mathrm{E}_\mathrm{loc} \tag{6.13}$$

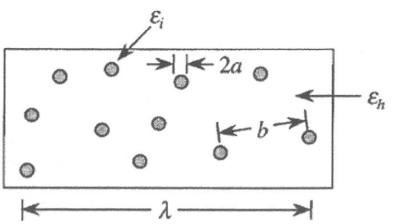

Fig. 6.3 Maxwell-Garnett geometry (From Ref. [24])

where 'a' is the nanoparticle radius and $\mathbf{E_{loc}}$ is the local field experienced by the nanoparticle. For sparse, randomly distributed dipoles, the local field is given by the Lorentz relation:

$$E_{loc} = E_0 + \frac{4\pi}{3\,\epsilon_h} P \tag{6.14}$$

Although only metallic particles are considered, the derivation is valid in general, i.e., the constituents may be pure dielectrics as well. The above mentioned local electric field value depends on the polarization of the surrounding medium and also on the applied field, and it is not the same as the macroscopic electric field appearing in Maxwell's equations. Local-field effects play a role in each of the composite geometries to be considered, and is quite significant in nonlinear effective medium theories since the local-field correction factor appears multiple times in expressions for the nonlinear susceptibilities.

6.6.2 *Bruggeman Geometry*

This model assumes that grains of two or more materials are randomly interspersed (Fig. 6.4). The intermixed components possess different or enhanced linear and nonlinear optical properties. To analyze composites of Bruggeman geometry, one considers a single grain within the whole. Grains of each type of constituent material will surround this grain. The grains are considered to be surrounded by a material of uniform dielectric constant given by that of the effective medium. If we take the grain to be spherical, we may solve for the internal electric field due to a uniform applied field E_0: The linear optical properties are described by the equation,

$$E_i = \frac{3\,\epsilon_{eff}}{\epsilon + 2\,\epsilon_{eff}} E_0 \tag{6.15}$$

which leads to a displacement field of the form

$$D_i = \epsilon_i \frac{3\,\epsilon_{eff}}{\epsilon_i + 2\,\epsilon_{eff}} E_0 \tag{6.16}$$

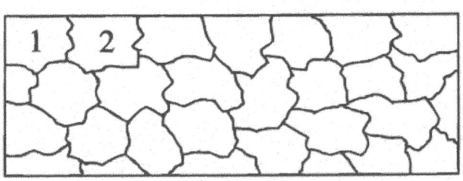

Fig. 6.4 Bruggeman (interspersed) geometry (From Ref. [24])

This theory will be applicable for materials in which all components occupy large volume fractions of the whole. An important feature of this model is that, as the volume fraction of one constituent increases from a small value, it will reach a point at which the grains begin to join and form continuous threads throughout the composite. At this stage, the Bruggeman theory accounts superbly over the Maxwell-Garnett model for the inclusion of conductivity of a metal/insulator composite and the behavior near the surface plasmon resonance of metal particles in a dielectric [25]. At very low volume fractions of the metallic constituent, the predictions of the two models are virtually identical. However, as the volume fraction increases the Maxwell-Garnett model continues to predict a sharp resonance, whereas the Bruggeman model predicts a broadening and weakening of the resonance.

6.6.3 *Layered Geometry*

Another composite geometry is that of alternating layers of two or more materials, shown in Fig. 6.5. Such a composite is considered to be anisotropic and uniaxial because the optical properties measured by using electric fields polarized parallel to the layers will be typically different from those for electric fields polarized perpendicular to the layers. To develop an effective medium theory, it is assumed that each layer is much thinner than an optical wavelength. For electric fields parallel to the layers the field is continuous across the boundaries of each layer, and the effective linear dielectric constant and nonlinear susceptibilities can be written as averages of the constituents:

$$\epsilon_{II} = f_1 \epsilon_1 + f_2 \epsilon_2 \tag{6.17}$$

and

$$\chi^{(2)}_{sum} = f_1 \chi^{(2)}_1 + f_2 \chi^{(2)}_2 \tag{6.18}$$

Here f represents the volume fill fraction of the nanoparticles or layers. When the electric field is polarized perpendicular to the layers, more interesting effects occur. In this case, the field is continuous across the layer boundaries, and the electric field is

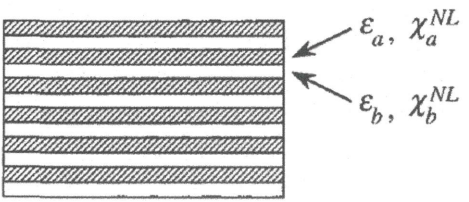

Fig. 6.5 Layered geometry (From Ref. [24])

distributed non-uniformly between the layers, resulting in the nonlinear susceptibility becoming more complicated.

6.6.4 *Fractal Structures*

Another type of nanocomposite is formed when one of the constituents forms fractal structures within the whole. For example, one constituent could consist of metal spheres or dielectric nanoparticles that clump together forming aggregates with a fractal dimension. The mode in which the clusters form will affect their fractal dimension, which in turn affects the nonlinear optical properties. Since fractals do not possess translational symmetry, they cannot propagate pure traveling waves. However, local-field effects can be strong in fractal structures. Due to their geometry localized field excitations arise, which may lead to regions of enhanced absorption [26]. The scattering cross section is found to increase with the number of monomers until the size of the fractal becomes comparable to an optical wavelength, when saturation occurs [27]. Hui and Stroud analyzed the linear properties of fractal composites using a three-dimensional differential effective medium approach on self-similar clusters [28]. The approach of Shalaev and Stockman to fractal composites used a binary approximation, which considers the dipole-dipole coupling of the monomer to its nearest neighbor. The effect of the other monomers was found out by using a modified Lorentz local field [29].

Determination of the nonlinear optical properties of fractal composites is a more difficult task. Butenko et al. used the binary approximation to determine enhancement factors arising from the nonlinearities of impurities linked to the fractal for various nth-order nonlinear processes [30]. This factor could be very large due to the strong localized fields within the fractal structure. A number of other approximations also can be found in literature for the optical properties of fractal structures.

6.7 Optical Nonlinearity Measurements in Nanomaterials

Several authors have reported nonlinear optical properties of nanomaterials in literature, and a selected few are given below. Experimental results are broadly classified into second order and third order effects. The key requirements for practical nonlinear optical materials are fast response time, strong nonlinearity, broad wavelength range, low optical loss, high power handling, and ease of integration into an optical system. Since substantial advances have been made during the last 10 years in the design of plasmonic and carbon based nanomaterials, we focus on those materials below.

6.7.1 *Second Order Nonlinearities*

Second order nonlinearities occur in crystalline media with a non-centrosymmetric structure. NLO crystals such as potassium dihydrogen phosphate (KDP), lithium niobate ($LiNbO_3$), and super lattices grown by molecular-beam epitaxy (MBE) are readily available, but it is difficult to incorporate these materials into most photonic platforms. So, there is substantial current research interest on nonlinear optical nanomaterials for harmonic generation and frequency conversion applications.

Second harmonic generation (SHG) was first demonstrated by Franken et al. at the University of Michigan in 1961. They focused a ruby laser beam (694 nm) into a quartz crystal, and the output measured through a spectrometer and recorded on photographic paper revealed the production of light at 347 nm [31]. There is strong recent interest in the optical response of metal nanoparticles in view of the local field enhancements [32]. Giant local field enhancement factors of the order of 10^6 have been predicted, which are significant for nonlinear optical processes such as SHG and THG in nanomaterials.

An overview of how the second order NLO properties of nanomaterials vary with size, symmetry, and shape is given in the review by Ray [33]. In addition, the emergence of second order NLO nanomaterials for the development of nanomaterial based optical technology has also been discussed. The advancements in the design of nanomaterials of different sizes and shapes for NLO is highlighted. SHG from metal nanoparticles is typically attributed to electric dipole excitations at their surfaces caused by strong polarization, but nonlinearities involving higher multipole effects may also be significant due to strong nanoscale gradients in the local material properties and fields. The paper also summarizes recent advancements on the development of a nanomaterials based NLO assay for monitoring chemical processes, and sensing biomolecules and toxic metals [33] (Fig. 6.6).

Nonlinear plasmonic effects have applications including switching and modulation of optical signals, frequency conversion, and soliton generation. Tuning of plasmonic resonances in metamaterials and utilization of their properties will be important for the development of next-generation, low-power, all optical switches and all-optically-tunable plasmonic devices. Similarly, the advantages of GaAs nanowires

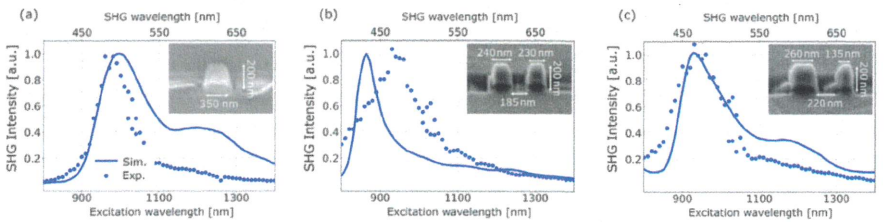

Fig. 6.6 Measured and calculated second harmonic emission of **a** single **b** symmetric dimer **c** asymmetric dimers of some III–IV semiconductor nanorods. SEM images of the corresponding structures are provided in the inset (from Ref. [34])

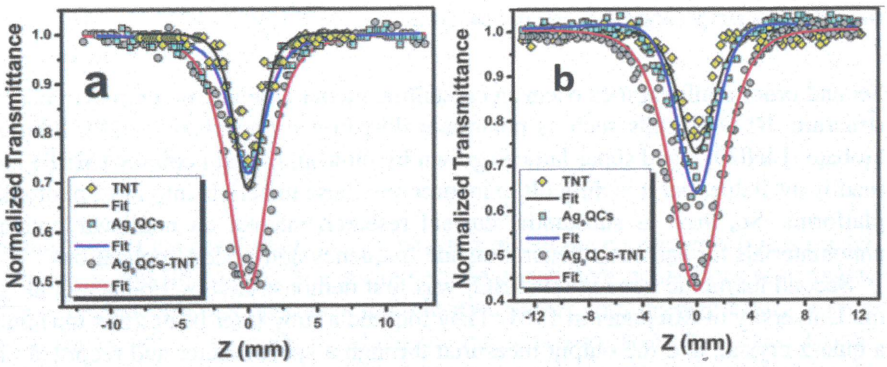

Fig. 6.7 Open aperture Z-scan curves measured for TNT, Ag9QCs and Ag9QCs-TNT. **a** Excitation by ultrashort (100 fs) laser pulses at 800 nm. Laser pulse energy used is 8 μJ. **b** Excitation by short (5 ns) laser pulses at 532 nm. Laser pulse energy used is 30 μJ (from Ref. [46])

have been used recently to design and fabricate nonlinear nanoantennas with controllable emission of the second harmonic (SH) radiation (Fig. 6.7) [34]. This work can be applied for the development of new types of nonlinear photonic components, which can be useful in integrated photonic circuits.

Applications of graphene in nonlinear optics continue to be explored vigorously. Second-order-nonlinear optical effects of graphene, particularly SHG, have been investigated theoretically [35–38]. Dean et al. have experimentally demonstrated SHG in graphene and multilayer graphite films mounted on a SiO_2/Si substrate using 150 fs laser pulses at 800 nm [39]. From numerical modeling, Gao et al. have demonstrated that phase matching and SHG can be realized in a pair of parallel graphene nanowires. The authors conclude that phase matching can be achieved between the hybridized modes by tuning the spacing of the nanowire pair. In order to achieve the largest conversion efficiency, one needs to choose the appropriate modes, and to further enhance the nonlinearity the nanowire radius should be decreased. Additionally, electromagnetic field enhancement due to surface plasmons will occur near the nanowires, further boosting the nonlinearity [40]. For frequency doubling applications, the abundance of polarizable π electrons in graphene could yield structures with large first hyperpolarizability if the centrosymmetry is broken. From computational modeling it has been shown that graphene nanoribbon (GNR) can be used as an excellent conjugated bridge in a donor–conjugated bridge–acceptor (D–B–A) framework to design high-performance second-order nonlinear optical materials [40].

6.7.2 *Third Order Nonlinearities*

Third-order nonlinear optical interactions (i.e., those described by a $\chi^{(3)}$ susceptibility) can occur for both centrosymmetric and non-centrosymmetric media. Symmetry-permitted third-order optical nonlinearity is remarkably strong in plasmonic, dielectric, carbon and graphene nanomaterials, leading to effects like saturable absorption, reverse saturable absorption and wave mixing. Third-order optical nonlinearity plays a key role in nonlinear photonic devices. Materials which are currently relevant to third order nonlinear optics can be divided into five main categories, viz. metal nanoparticles, dielectric nanoparticles, carbon and graphene-based materials, and epsilon-near-zero (ENZ) materials.

6.7.2.1 Metal Nanoparticles

Regardless of the emission wavelength, ultrafast lasers utilize a mode-locking procedure, whereby a nonlinear optical component, called a saturable absorber, transforms the continuous-wave output into a train of ultrafast optical pulses [41, 42]. There are reports on the observation of saturable absorption (SA) in plasmonic metal nanoparticles, even though switching to reverse saturable absorption (RSA) has been observed at higher intensities [43, 44].

Noble metal nanostructures embedded in transparent dielectric matrices have been attracting significant attention towards all-optical signal processing device applications. This is because of the large third-order nonlinear optical properties caused by the phenomena of surface plasmon resonance (SPR) and quantum size effect. Silver NPs experience a lower (compared to what?) intrinsic loss of plasmonic energy at visible frequencies. SA at 532 nm has been observed at low input irradiances in Ag nanodots prepared by pulsed laser deposition [45]. Kishore et al. [46] has studied enhanced nonlinear absorption of Ag_9QCs-TNT composite compared to its pristine precursors, Ag_9QC and TNT. Nonlinear absorption is attributed mainly to excited state and free carrier absorption phenomena for 5 ns excitation, while two-photon absorption should be more prominent for 100 fs excitation. α_2 measured for Ag_9QCs-TNT for ns excitation is 2.7×10^{-10} m/W, while that for fs excitation is 1.6×10^{-14} m/W. These values show that Ag_9QCs-TNT an excellent material for passive optical limiting device applications. Several studies are available in literature on Ag nanocomposites, some of which are shown in Table 6.1.

Gold metamaterials are the next promising candidates for NLO, which can be potentially used for fabricating optical sensors and saturable absorbers. In the presence of external fields, they can control material properties as well [47]. Gold nanorods (GNRs) have been used as saturable absorbers for passive mode-locking at 1 μm wavelength. Absorption at the longitudinal surface plasmon resonance of GNRs is used to induce mode-locking. By using GNR film, stable passive mode-locking has been demonstrated at 1039 nm in an ytterbium-doped fiber laser cavity pumped by a 980 nm laser diode [48, 49]. Gold-nanospheres (GNS) also exhibit

Table 6.1 NLO investigations in some nanomaterials

Nanostructure	Wavelength (nm) (λ_{probe})/Pulse duration	Reference
Silver nanoparticles	532 nm, 6 ns	[93]
	1200 nm, 100 fs	[94]
	532 nm, 16 ns	[95]
	795 nm, 110 fs	[96]
	532 nm, 5 ns 800 nm, 100 fs	[97]
	532 nm, 5 ns	[98]
	532 nm, 5 ns	[99]
	800 nm, 190 fs	[100]
	800 nm, 100 fs	[101]
Gold nanoparticles	800 nm, 100 fs	[102]
	1500 nm, 70 fs	[103]
	532 nm, 26 ps	[104]
	800 nm, 150 fs	[105]
	532 nm, 8 ns	[106]
	532 nm, 35 ps	[76]
	800 nm, 35 fs	[107]
	532 nm, 5 ns	[44]
	532 nm, 7 ns	[108]
	800 nm, 60 fs	[109]
Dielectric materials Silicon composites	1200 nm, 240 fs	[110]
	1100–1500 nm, 100 fs	[111]
	532 nm, 8 ns	[112]
	772 nm, 275 fs 1030 nm, 140 fs 1550 nm, 97 fs	[113]
Two dimensional materials WS_2/MoS_2 composites	1030 nm, 340 fs 800 nm, 40 fs 515 nm, 340 fs	[114]
WS_2	800 nm, 100 fs	[115]
MoS_2	532 nm, 8 ns	[81]
Carbon/graphene based materials	400 nm–700 nm, 100 fs	[116]
	532 nm, 5 ns, 35 ps	[117]
	1053 nm, 75 ps	[118]
	400 nm, 800 nm, 1562 nm, 565 fs	[119]
	1030 nm, 340 fs	[120]
Epsilon zero materials	1240 nm, 150 fs	[121]
	720 nm, 200 fs	[122]

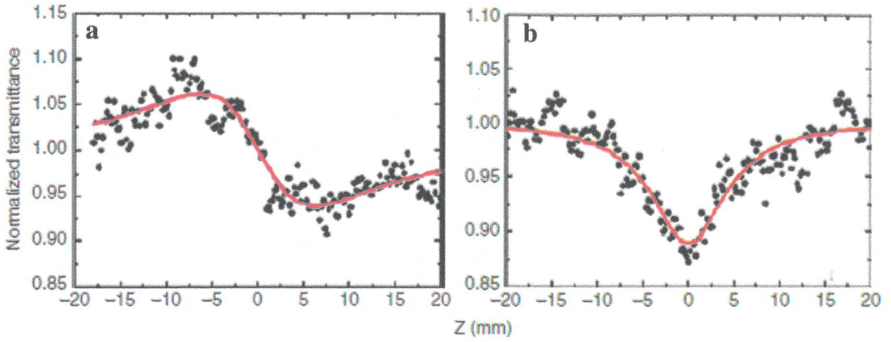

Fig. 6.8 Closed and open aperture Z-scan measurements of a gold metasurface at 1500 nm, using 70 fs, 1 kHz laser pulses obtained from an optical parametric amplifier. The peak intensity used is 45 GW/cm^2 (from Ref. [90])

saturable absorption behavior. An all-fiber passively Q-switched erbium doped fiber laser (EDFL) using GNS based saturable absorber (SA) with evanescent field interaction has been demonstrated [50]. Closed and open aperture Z-scan measurements carried out on a gold metasurface using 70 fs, 1500 nm laser pulses are shown in Fig. 6.8. From the data, the nonlinear optical parameters are calculated to be $\alpha_2 = 3 \times 10^{-6}$ cm/W and $n_2 = -1.05 \times 10^{-10}$ cm^2/W, respectively. Measurements carried out at 800 nm gave values of $\alpha_2 = -0.90 \times 10^{-4}$ cm/W and n2 = -7.90×10^{-9} cm^2/W. More detailed studies on gold nanocomposites are mentioned in Table 6.1 for further reference.

Other than Ag and Au nanoparticles, studies in some other promising metal nanoparticles such as Zn, Ni, and Al Ti, derivatives also are available in literature [51–54].

6.7.2.2 Dielectric Nanoparticles

Silicon-based optical devices have received much attention because of their potential applications in high-speed signal processing and no-chip communications [55]. A major advantage of silicon photonic devices is that they can be produced efficiently because of the highly advanced silicon processing technology, permitting low-cost, large-volume electronic circuit production. Silicon photonics makes optical devices compatible with CMOS technology, allowing for on-chip integration [56].

The nonlinear optical response of nc-Si/SiO_2 multilayers excited by ps and fs laser pulses, studied by Zhang et al. [57], is shown in Fig. 6.9. When the sample is excited by picosecond laser pulses absorption saturation is observed ($\alpha_2 = -3.1 \times 10^{-6}$ cm/W^{-1}), with a nonlinear refraction coefficient of $n_2 = -1.3 \times 10^{-10}$cm^2 W^{-1}. Absorption saturation can be attributed to the single photon transition process between the valence band and the interface state, while negative nonlinear refraction is due to the free carrier dispersion effect. However, when the multilayers are excited

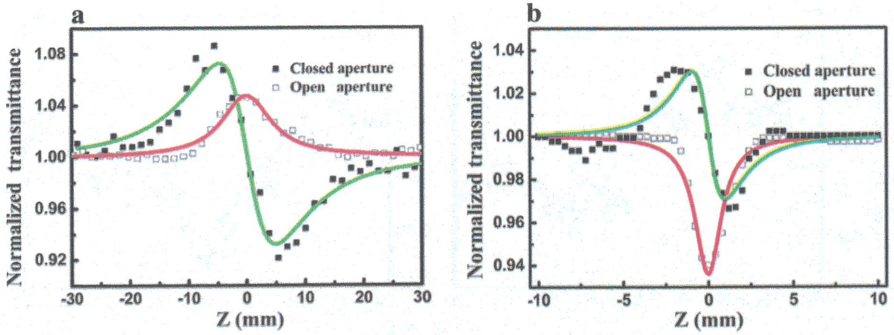

Fig. 6.9 Z-scan curves of nc-Si/SiO_2 multilayer sample in the closed aperture (full square) and open aperture (empty square) configurations. **a** $\lambda = 1064$ nm, $t_p = 25$ ps, laser intensity $I_0 = 1.18 \times 10^{10}$ W/cm^2. **b** $\lambda = 800$ nm, $t_p = 50$ fs, $I_0 = 3.54 \times 10^{11}$ W/cm^2. Solid curves are theoretical fits to the experimental data (from Ref. [91])

by femtosecond laser pulses, reverse saturation absorption is observed ($\alpha_2 = 1.1 \times 10^{-7}$ cm W^{-1}) while the sign of nonlinear refraction is unchanged ($n_2 = -1.5 \times 10^{-12}$ cm^2 W^{-1}). The difference in the free carrier densities generated by the different pulse durations play a significant role in the observed sign reversal of the absorptive nonlinearity. Variations in the nonlinear absorption and refraction responses of these multilayers during the transition from the amorphous to nanocrystalline phase also have been studied under femtosecond excitation at 800 nm by Zhang et al. [58]. These studies indicate the possible application of nc-Si/SiO_2 multilayers in photonic devices such as optical switches and Q-switch lasers.

6.7.2.3 Carbon and Graphene Based Materials

Carbon nanotubes and graphene have developed as promising materials for use in ultrafast fiber lasers [59, 60]. Their exceptional electrical and optical properties empower them to be utilized as saturable absorbers with fast responses and broadband operation, which can be effectively coordinated in fiber lasers. Assemblies of carbon nanotubes in suspension or in polymeric matrices can be used as saturable absorbers for near infrared light [61–63]. Currently used semiconductor saturable absorber mirrors have a thin tuning range, and require complex fabrication and packaging. A straightforward, cost-effective alternative is to utilize single-walled carbon nanotubes (SWNTs). Broadband tunability is achievable by utilizing SWNTs with a wide width distribution [64]. Since graphene–polymer composites are adaptable, they can be effortlessly incorporated into a number of photonic frameworks. So far, graphene–polymer composites [65, 66], CVD-grown films [67], functionalized graphene, and reduced graphene oxide flakes have been used for ultrafast lasers as saturable absorbers [68, 69]. Graphene-based ultrafast lasers and carbon-nanotube-based devices are discussed in the review paper by Bonaccorso et al. [70]. Martinez

and Sun have demonstrated that nanotube and graphene nanocomposites are efficient saturable absorbers for fiber lasers. They emphasize that the easy fabrication and integration of SAs based on CNTs and graphene and their broad operation bandwidths are extremely valuable for various new fiber mode-locked lasers operating at broad wavelength ranges [71]. Saturable absorption has been shown in MoS_2, graphene and MoS_2/graphene nanocomposites in a number of solvents, as depicted in Fig. 6.10 [72].

Similarly, there is substantial enthusiasm for the study of optical limiting for protecting optical sensors and human eyes from intense light, as retinal harm can happen when intensities surpass a specific threshold. Passive optical limiters, which

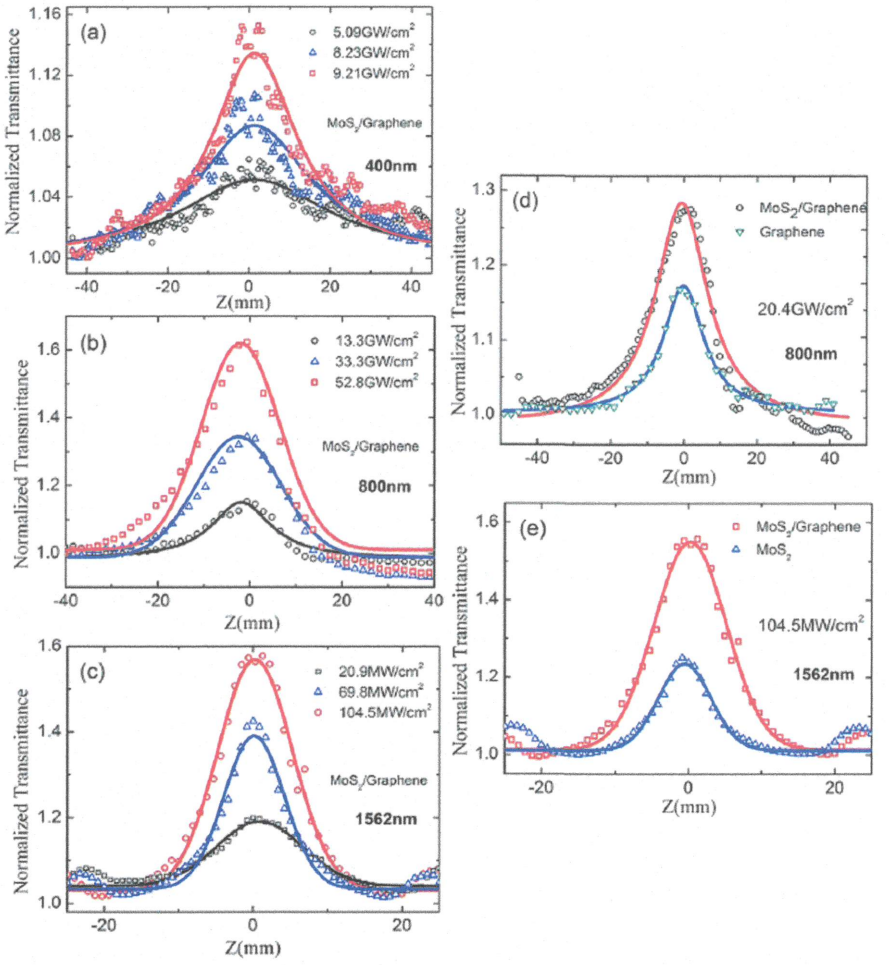

Fig. 6.10 Saturable absorption measured in MoS_2, graphene and MoS_2/graphene nanocomposites for different input fluences and wavelengths (from Ref. [72])

utilize nonlinear optical phenomena, can possibly be small, cheap and straightforward in design. However, no passive optical limiter has yet been designed which secures human eyes and common optical sensors from damage over the entire visible and near-infrared wavelength range. Reverse saturable absorption is a major physical mechanism which results in the optical limiting effect.

Sun et al. has reviewed optical limiters based on different classes of nanomaterials, including metal and semiconductor nanoparticles and nanoscale carbon materials [73]. They observe that carbon nanomaterials, ranging from carbon nanoparticles to fullerenes and to carbon nanotubes, are among the best optical limiters for nanosecond laser pulses. Philip and colleagues have reported that ligand-protected/capped gold and silver nanoclusters and their alloys are good optical limiters for nanosecond and picosecond laser pulses [44, 74–76]. Broad optical limiting in exfoliated graphene has been reported [45, 77, 78], and functionalized graphene dispersions are better than C_{60} for optical limiting [79, 80]. Carbon-based materials (for example, carbon-black dispersions, and CNTs, fullerenes and their derivatives) [81] have good optical limiting performance, in particular for nanosecond pulses at 532 and 1064 nm. The combination of plasmonic metal nanoparticles with carbon-based nanoparticles or different composites of graphene nanoparticles exhibit enhanced optical limiting [82–86] as seen from Fig. 6.11. Nonlinear absorption studies of different carbon-based materials/graphene composites are shown in Table 6.1.

6.7.2.4 Epsilon-Near-Zero (ENZ) Metamaterials

Recently, it has been found that materials with very small dielectric permittivity show efficient nonlinear optical behavior. These are generally known as epsilon-near-zero (ENZ) materials. These media can produce substantial enhancements to the local electric field, and high frequency conversion efficiencies [87, 88]. Transparent conducting oxides (TCO) have become important candidates in this category due to their unique NLO properties at epsilon-near-zero wavelengths. TCOs such as Indium-Tin-Oxide (ITO) exhibit a vanishing real part of the permittivity in the near-infrared where the group velocity of light decreases considerably and causes a strong light-matter interaction. A modest field intensity enhancement in the ITO film can lead to a large enhancement of nonlinear refraction coefficient (n_2) at the ENZ wavelengths. The hot-electron–induced optical nonlinearity of ITO films at ENZ wavelengths differs from that of noble metals under infrared irradiation in two ways. First, for a given change in permittivity, the nonlinear change in refractive index is always larger in the ENZ region than that in non-ENZ regions. Second, the free-electron heat capacity of ITO is more than one order of magnitude smaller than that of a noble metal such as gold. Thus, the increase in the free-electron temperature compared to the Fermi temperature and the consequent change in refractive index of ITO is much larger. ITO film shows an extremely large ultrafast third-order nonlinearity at ENZ wavelengths, and it can attain an optically induced change in the refractive index that is unprecedentedly large.

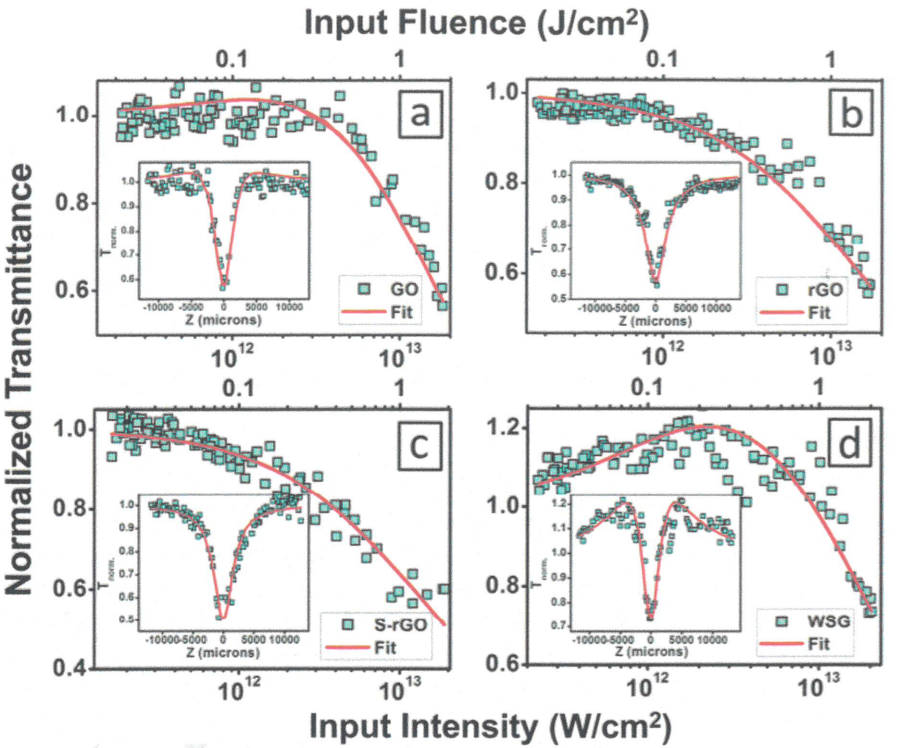

Fig. 6.11 Nonlinear transmission curves obtained from open aperture Z-scans (insets) measured for GO, rGO, S-rGO, and water soluble graphene (WSG), for 800 nm, 100 fs laser pulse excitation. Laser pulse energy used is 10 μJ (from Ref. [84])

ITO based sandwich structures with the insertion of silver (ITO/Ag/ITO) show large nonlinear optical enhancement of both nonlinear refraction and saturable absorption. The nonlinear refractive index ($n_2 = 15.43 \times 10^{-16}$ m^2/W) and nonlinear absorption coefficient ($\beta = -648 \times 10^{-11}$ m/W) measured for an ITO/Ag/ITO sandwich are found to be about 18 and 16 times greater than that measured for single-layer ITO, respectively, as shown in Fig. 6.12. The observed optical nonlinearity enhancement can be attributed to the inclusive effect of the increase of carrier concentration and local field enhancement induced by SPR in the sandwiches. Some of the investigations carried out with ITO hybrid metamaterials are shown in Table 6.1.

6.7.3 Applications of Optical Nonlinearity in Nanoparticles

There are different ways to classify NLO materials for different applications. The criteria can be the order of the nonlinearity, the nature of the NLO interaction, or some

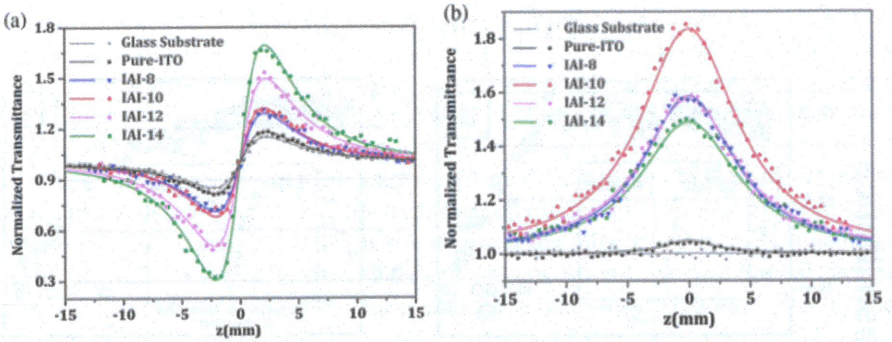

Fig. 6.12 Nonlinear optical responses of glass substrate, Pure-ITO, and ITO-Ag (IAI) sandwiches with various Ag insertion thicknesses, measured by Z-scan (from Ref. [92])

unique characteristics of the particular materials. Practically, for a given application, several potential NLO materials may be available.

Second-order NLO materials are used for the generation of new frequencies by means of SHG, sum- and difference-frequency mixing or optical parametric oscillation (OPO) [123]. In general, while several materials may be used for the production of radiation at a given wavelength, often one or two of them are better suited for a given process compared to the others. The second generation of NLO materials have been mainly organics, including organic single crystals, organic-inorganic single crystals, chromophore-hosted polymers and Langmuir-Blodgett (LB) films [124]. Third-order NLO materials comprise semiconductors, quantum confined semiconductors (quantum wells, quantum wires and quantum dots), metal particles, organics (crystals, polymers, and guest-host systems doped with active molecules) and inorganic glasses.

The development of different nanostructures has given a boost to nonlinear photonics, which has become an important research direction. Optical modulators, optical polarizers, optical switchers, and all-optical devices are part of nonlinear photonics research. The development of 2D layered materials was crucial in this regard, laying a good foundation for practical applications [125].

Another developing field of interest is nonlinear microscopy for biomedical applications using nanoparticles. Confocal fluorescence microscopy is a powerful tool for visualizing biological processes, but conventional laser scanning confocal microscopy cannot resolve structures below the diffraction limit of light. Recent advances in far-field super-resolution techniques have demonstrated that the diffraction limit can be overcome through a combination of smart optical design, novel photon excitation and detection schemes, the selection of specialized fluorescent labels, and dedicated data processing. Such nonlinear techniques can be sandwiched to the existing techniques to optimize the resolution of microscopy [126]. For instance, photon avalanche in lanthanide doped nanoparticles is useful for super-resolution imaging [127]. Developments are still going on in super-resolution microscopy to find better and faster methods for different applications [128]. Another

promising line of work is optical nonlinear endoscopic tweezers, which is potentially an unprecedented tool for precisely specifying the location and dosage of drug particles, and for rapidly uploading metallic nanoparticles to individual cancer cells for treatment via two-photon absorption [129]. This technique allows an operation wavelength at the center of the transmission window of human tissue. Several other investigations also are ongoing on biomedical diagnostics and therapy using nonlinear optical responses of novel nanostructures [130, 131].

6.8 Conclusion

Large optical nonlinearities exhibited by dielectric, plasmonic and carbon-based nanomaterials hold great technological promise because of the possibility to modify their electronic and optical properties through material engineering. The emergence of metamaterials having novel structure-dependent properties has led to advanced research in nonlinear optics. Strong light-matter coupling in metamaterials produces novel linear and nonlinear optical properties. The development of these new materials in the field of photonics will continue to deepen, laying a good foundation for their practical applications. Selective combinations of dielectric, plasmonic and epsilon-near-zero materials is a very promising direction for further growth of nonlinear optics. These materials can be exploited for the fabrication of many key-devices for the telecom industry such as switches, routers, and wavelength converters. They are also attractive for applications such as photonic devices, sensing, terahertz imaging, and optical fibers. NLO nanomaterials can be used in the solution, film and solid forms, and a large number of chemical permutations and combinations are possible. In the medical field, nonlinear microscopy and nonlinear endoscopic tweezers hold great promise for diagnostics and treatment.

References

1. P.A. Franken, A.E. Hill, C.W. Peters, G. Weinreich, Phys. Rev. Lett. **7**, 118 (1961)
2. N. Bloembergen, Rev. Mod. Phys. **54**, 685 (1982)
3. R.W. Boyd, *Nonlinear Optics* (Academic Press, 2003)
4. P. Paufler, Cryst. Res. Technol. **26**, 802 (1991)
5. P.M. Rentzepis, Y. Pao, Appl. Phys. Lett. **5**, 156 (1964)
6. P.N. Prasad, *Nanophotonics* (Wiley, 2004)
7. B. Guo, Q.-L. Xiao, S.-H. Wang, H. Zhang, Laser Photonics Rev. **13**, 1800327 (2019)
8. A.K. Geim, K.S. Novoselov, Nat. Mater. **6**, 183 (2007)
9. J. Wang, Y. Chen, W.J. Blau, J. Mater. Chem. **19**, 7425 (2009)
10. R. Saito, G. Dresselhaus, M.S. Dresselhaus, Phys. Rev. B **61**, 2981 (2000)
11. G.Y.S.A.M. Nemilentsau, A.A. Khrushchinsky, S.A. Maksimenko, Carbon N. Y. **44**, 2246 (2006)
12. A.S.L. Gomes, M. Maldonado, L.S. de Menezes, L.H. Acioli, C.B. de Araújo, J. Dysart, D. Doyle, P. Johns, J. Naciri, N. Charipar, J. Fontana, Nanophotonics **9**(4), 725 (2020)

13. O. Reshef, I. De Leon, M. Zahirul Alam, R.W. Boyd, Nature Rev. Mater. **4**, 535 (2019)
14. M. Silveirinha, N. Engheta, Tunneling of electromagnetic energy through subwavelength channels and bends using ϵ-near-zero materials. Phys. Rev. Lett. **97**, 157403 (2006)
15. R.L. Sutherland, *Handbook of Nonlinear Optics* (CRC Press, 2003)
16. A. Hermans, C. Kieninger, K. Koskinen, A. Wickberg, E. Solano, J. Dendooven, M. Kauranen, S. Clemmen, M. Wegener, C. Koos, R. Baets, Sci. Rep. **7**, 44581 (2017)
17. S.K. Kurtz, T.T. Perry, J. Appl. Phys. **39**, 3798 (1968)
18. S. Chen, K.F. Li, G. Li, K.W. Cheah, S. Zhang, Light Sci. Appl. **8**, 17 (2019)
19. G. Berkovic, G. Meshulam, Z. Kotler, J. Chem. Phys. **112**, 3997 (2000)
20. K.Y. Suponitsky, S. Tafur, A.E. Masunov, J. Chem. Phys. **129.4**, 044109 (2008)
21. M. Sheik-Bahae, A.A. Said, T.-H. Wei, D.J. Hagan, E.W. Van Stryland, IEEE J. Quantum Electron. **26**, 760 (1990)
22. D.S. Correa, L.D. Boni, L. Misoguti, F.E.H.I. Cohanoschi, C.R. Mendonca, Opt. Commun. **277**, 440 (2007)
23. B. Gu, J. Wang, J. Chen, Y.-X. Fan, J. Ding, H.-T. Wang, Opt. Express **13**, 9230 (2005)
24. R.J. Gehr, R.W. Boyd, Chem. Mater. **8**, 1807 (1996)
25. P. Sheng, Phys. Rev. Lett. **45**, 60 (1980)
26. V.A. Markel, V.M. Shalaev, E.B. Stechel, W. Kim, R.L. Armstrong, Phys. Rev. B **53**, 2425 (1996)
27. M.V. Berry, I.C. Perciva, Opt. Acta **33**, 57728 (1986)
28. P.M. Hui, D. Stroud, Phys. Rev. **33**, 2163 (1986)
29. V.M. Shalaev, M.I. Stockman, Z. Phys. D: At. Mol. Clust. **10**, 71 (1988)
30. A.V. Butenko, V.M. Shalaev, M.I. Stockman, Zeitschrift Phys. D Atoms, Mol. Clust. **10**, 81 (1988)
31. M. Chandra, P.K. Das, Chem. Phys. **358**, 203 (2009)
32. M. Kauranen, A.V. Zayats, Nat. Photonics **6**, 737 (2012)
33. P.C. Ray, Chem. Rev. **110**, 5332 (2010)
34. G. Saerens, I. Tang, M.I. Petrov, K. Frizyuk, C. Renaut, F. Timpu, M. Reig Escalé, I. Shtrom, A. Bouravleuv, G. Cirlin, R. Grange, Laser Photonics Rev. **14**(9), 2000028 (2020)
35. J.J. Dean, H.M. van Driel, Phys. Rev. B **82**, 125411 (2010)
36. S.A. Mikhailov, Phys. Rev. B **84**, 45432 (2011)
37. M.M. Glazov, JETP Lett. **93**, 366 (2011)
38. S. Wu, L. Mao, A.M. Jones, W. Yao, C. Zhang, X. Xu, Nano Lett. **12**, 2032 (2012)
39. J.J. Dean, H.M. van Driel, Appl. Phys. Lett. **95**, 261910 (2009)
40. Y. Gao, I.V. Shadrivov, Sci. Rep. **6**, 38924 (2016)
41. Z.-J. Zhou, X.-P. Li, F. Ma, Z.-B. Liu, Z.-R. Li, X.-R. Huang, C.-C. Sun, Chem. A Eur. J. **17**, 2414 (2011)
42. Z. Kang, Q. Li, X.J. Gao, L. Zhang, Z.X. Jia, Y. Feng, G.S. Qin, W.P. Qin, Laser Phys. Lett. **11**, 35102 (2014)
43. Z. Kang, Y. Xu, L. Zhang, Z. Jia, L. Liu, D. Zhao, Y. Feng, G. Qin, W. Qin, Appl. Phys. Lett. **103**, 41105 (2013)
44. R. Philip, G.R. Kumar, N. Sandhyarani, T. Pradeep, Phys. Rev. B **62**, 13160 (2000)
45. R. Philip, P. Chantharasupawong, H. Qian, R. Jin, J. Thomas, Nano Lett. **12**, 4661 (2012)
46. U. Gurudas, E. Brooks, D.M. Bubb, S. Heiroth, T. Lippert, A. Wokaun, J. Appl. Phys. **104**(7), 073107 (2008)
47. K. Sridharan, P. Sankar, R. Philip, Opt. Mater. **94**, 53–57 (2019)
48. A.S. Gomes, M. Maldonado, L.D.S. Menezes, L.H. Acioli, C.B. de Araújo, J. Dysart, D. Doyle, P. Johns, J. Naciri, N. Charipar, J. Fontana, Nanophotonics **9**(4), 725–740 (2020)
49. Z. Kang, Q. Li, X.J. Gao, L. Zhang, Z.X. Jia, Y. Feng, G.S. Qin, W.P. Qin, Laser Phys. Lett. **11**(3), 035102 (2014)
50. J. Lee, J. Koo, J.H. Lee, Laser Phys. Lett. **14**(9), 090001 (2017)
51. D. Fan, C. Mou, X. Bai, S. Wang, N. Chen, X. Zeng, Opt. Express **22**(15), 18537–18542 (2014)
52. R. Sreeja, J. John, P.M. Aneesh, M.K. Jayaraj, Opt. Commun. **283**(14), 2908–2913 (2010)

53. E. Ramya, M.V. Rao, L. Jyothi, D.N. Rao, J. Nanosci. Nanotechnol. **18**(10), 7072–7077 (2018)
54. R. Kuladeep, L. Jyothi, P. Prakash, S. Mayank Shekhar, M. Durga Prasad, D. Narayana Rao, J. Appl. Phys. **114**(24), 243101 (2013)
55. R. Sato, S. Ishii, T. Nagao, M. Naito, Y. Takeda, ACS Photonics **5**(9), 3452–3458 (2018)
56. B. Jalali, Silicon photonics: nonlinear optics in the midinfrared, Nat. Photonics, **4**, 506–508 (2010)
57. D.A.B. Miller, Optical interconnects to electronic chips. Appl. Opt. **49**(25), 59–70 (2010)
58. P. Zhang, D.K. Li, L.Y. Jiang, J. Xu, vol. 8, 012012 (IOP Publishing, 2017)
59. P. Zhang, X. Zhang, J. Xu et al., Tunable nonlinear optical properties in nanocrystalline Si/SiO_2 multilayers under femtosecond excitation. Nanoscale Res. Lett. **9**(1), 28 (2014)
60. H.A. Haus, IEEE J. Sel. Top. Quantum Electron. **6**, 1173 (2000)
61. S. Tatsuura, M. Furuki, Y. Sato, I. Iwasa, M. Tian, H. Mitsu, Adv. Mater. **15**, 534 (2003)
62. G. Rozhin, Y. Sakakibara, H. Kataura, S. Matsuzaki, K. Ishida, Y. Achib, A.C Madoka Tokumoto, Chem. Phys. Lett. **405**, 288 (2005)
63. F. Wang, A.G. Rozhin, V. Scardaci, Z. Sun, F. Hennrich, I.H. White, W.I. Milne, A.C. Ferrari, Nat. Nanotechnol. **3**, 738 (2008)
64. T. Hasan, Z. Sun, F. Wang, F. Bonaccorso, P.H. Tan, A.G. Rozhin, A.C. Ferrari, Adv. Mater. **21**, 3874 (2009)
65. Z. Sun, T. Hasan, F. Torrisi, D. Popa, G. Privitera, F. Wang, F. Bonaccorso, D.M. Basko, A.C. Ferrari, ACS Nano **4**, 803 (2010)
66. H. Zhang, Q. Bao, D. Tang, L. Zhao, K. Loh, Appl. Phys. Lett. **95**, 141103 (2009)
67. H. Zhang, D.Y. Tang, L.M. Zhao, Q.L. Bao, K.P. Loh, Opt. Express **17**, 17630 (2009)
68. H. Zhang, D. Tang, R.J. Knize, L. Zhao, Q. Bao, K.P. Loh, Appl. Phys. Lett. **96**, 111112 (2010)
69. Y.-W. Song, S.-Y. Jang, W.-S. Han, M.-K. Bae, Appl. Phys. Lett. **96**, 51122 (2010)
70. W.D. Tan, C.Y. Su, R.J. Knize, G.Q. Xie, L.J. Li, D.Y. Tang, Appl. Phys. Lett. **96**, 31106 (2010)
71. F. Bonaccorso, Z. Sun, T. Hasan, A.C. Ferrari, Nat. Photonics **4**, 611 (2010)
72. A. Martinez, Z. Sun, Nat. Photonics **7**, 842 (2013)
73. Y. Jiang, L. Miao, G. Jiang et al., Broadband and enhanced nonlinear optical response of MoS2/graphene nanocomposites for ultrafast photonics applications. Sci. Rep. **5**, 16372 (2015)
74. Y.-P. Sun, J.E. Riggs, K.B. Henbest, R.B. Martin, J. Nonlinear Opt. Phys. Mater. **9**, 481 (2000)
75. S. Kumar, M. Anija, N. Kamaraju, K.S. Vasu, K.S. Subrahmanyam, A.K. Sood, C.N.R. Rao, Appl. Phys. Lett. **95**, 191911 (2009)
76. R.T. Tom, A.S. Nair, N. Singh, M. Aslam, C.L. Nagendra, R. Philip, K. Vijayamohanan, T. Pradeep, Langmuir **19**, 3439 (2003)
77. B. Karthikeyan, M. Anija, R. Philip, Appl. Phys. Lett. **88**, 53104 (2006)
78. R.P.M. Anija, J. Thomas, N. Singh, S. Nair, R.T. Tom, T. Pradeep, Chem. Phys. Lett. **380**, 223 (2003)
79. J. Wang, Y. Hernandez, M. Lotya, J.N. Coleman, W.J. Blau, Adv. Mater. **21**, 2430 (2009)
80. Y. Xu, Z. Liu, X. Zhang, Y. Wang, J. Tian, Y. Huang, Y. Ma, X. Zhang, Y. Chen, Adv. Mater. **21**, 1275 (2009)
81. L.W. Tutt, A. Kost, Nature **356**, 225 (1992)
82. N. Mackiewicz, T. Bark, B. Cao, J.A. Delaire, D. Riehl, W.L. Ling, S. Foillard, E. Doris, Fullerene-functionalized carbon nanotubes as improved optical limiting devices. Carbon **49**(12), 3998–4003 (2011)
83. S. Perumbilavil, P. Sankar, T. Priya Rose, R. Philip, Appl. Phys. Lett. **107**, 51104 (2015)
84. Z.-B. Liu, Y.-F. Xu, X.-Y. Zhang, X.-L. Zhang, Y.-S. Chen, J.-G. Tian, J. Phys. Chem. B **113**, 9681 (2009)
85. K. Sridharan, P. Sreekanth, T.J. Park, R. Philip, J. Phys. Chem. C **119**, 16314 (2015)
86. R.P. Sreekanth Perumbilavil, K. Sridharan, D. Koushik , P. Sankar, V.P. Mahadevan Pillai, Carbon N. Y. **111**, 283 (2017)

87. B. Anand, A. Kaniyoor, S.S.S. Sai, R. Philip, S. Ramaprabhu, J. Mater. Chem. C **1**, 2773 (2013)
88. B.S. Kalanoor, P.B. Bisht, S. Akbar Ali, T.T. Baby, S. Ramaprabhu, J. Opt. Soc. Am. B **29**, 669 (2012)
89. A. Ciattoni, C. Rizza, E. Palange, Extreme nonlinear electrodynamics in metamaterials with very small linear dielectric permittivity. Phys. Rev. A **81**, 043839 (2010)
90. A. Ciattoni, C. Rizza, E. Palange, Transmissivity directional hysteresis of a nonlinear metamaterial slab with very small linear permittivity. Opt. Lett. **35**, 2130–2132 (2010)
91. M. Kyoung, M. Lee, Opt. Commun. **171**, 145–148 (1999)
92. L.d.S. Menezes, L.H. Acioli, M. Maldonado, et al., Large third-order nonlinear susceptibility from a gold metasurface far off the plasmonic resonance, J. Opt. Soc. Am. B **36**, 1485 (2019)
93. P. Zhang, X. Zhang, L. Peng et al., Interface state-related linear and nonlinear optical properties of nanocrystalline Si/SiO_2 multilayers. Appl. Surf. Sci. **292**(1), 262–266 (2014)
94. K. Wu, et al., Large optical nonlinearity of ITO/Ag/ITO sandwiches based on Z-scan measurement. Opt. Lett. **44.10**, 2490–2493 (2019)
95. R. Sathyavathi, M.B. Krishna, S.V. Rao, R. Saritha, D.N. Rao, Adv. Sci. Lett. **3**(2), 138–143 (2010)
96. A. Alesenkov, J. Pilipavičius, A. Beganskienė, R. Sirutkaitis, V. Sirutkaitis, Lith. J. Phys. **55**(2) (2015)
97. Y. Deng, Y. Sun, P. Wang, D. Zhang, H. Ming, Q. Zhang, In situ synthesis and nonlinear optical properties of Ag nanocomposite polymer films. Phys. E. **40**(4), 911–914 (2008)
98. R.A. Ganeev, M. Baba, A.I. Ryasnyansky, M. Suzuki, H. Kuroda, Opt. Commun. **240**(4–6), 437–448 (2004)
99. K. Sridharan, T. Endo, S.G. Cho, J. Kim, T.J. Park, R. Philip, Opt. Mater. **35**(5), 860–867 (2013)
100. K.B. Bhavitha, A.K. Nair, S. Perumbilavil, S. Joseph, M.S. Kala, A. Saha, R.A. Narayanan, N. Hameed, S. Thomas, O.S. Oluwafemi, N. Kalarikkal, Opt. Mater. **73**, 695–705 (2017)
101. P.B. Anand, C.S. Sandeep, K. Sridharan, T.N. Narayanan, S. Thomas, R. Philip, M.R. Anantharaman, Adv. Sci. Eng. Med. **4**(1), 33–38 (2012)
102. K. Liu, X. Xu, W. Shan, D. Sun, C. Yao, W. Sun, Opt. Mater. **99**, 109569 (2020)
103. K. Yu, Y. Yang, J. Wang, X. Tang, Q.H. Xu, G.P. Wang, Nanotechnology **29**(25), 255703 (2018)
104. J. Fontana, M. Maldonado, N. Charipar, et al., Opt. Express **24**, 27360–27370 (2016)
105. L.D.S. Menezes, L.H. Acioli, M. Maldonado, J. Naciri, N. Charipar, J. Fontana, D. Rativa, C.B. de Araújo, A.S. Gomes, J. Opt. Soc. Am. B **36**(6), 1485–1491 (2019)
106. O. Sánchez-Dena, P. Mota-Santiago, L. Tamayo-Rivera, E.V. García-Ramírez, A. Crespo-Sosa, A. Oliver, J.A. Reyes-Esqueda, Opt. Mater. Express **4**(1), 92–100 (2014)
107. E.C. Romani, D. Vitoreti, P.M. Gouvêa, P.G. Caldas, R. Prioli, S. Paciornik, M. Fokine, A.M. Braga, A.S. Gomes, I.C. Carvalho, Opt. Express **20**(5), 5429–5439 (2012)
108. S. Qu, C. Du, Y. Song, Y. Wang, Y. Gao, S. Liu, Y. Li, D. Zhu, Chem. Phys. Lett. **356**(3–4), 403–408 (2002)
109. A. Rout, G.S. Boltaev, R.A. Ganeev, Y. Fu, S.K. Maurya, V.V. Kim, K.S. Rao, C. Guo, Nanomaterials **9**(2), 291 (2019)
110. S. Edappadikkunnummal, S.N. Nherakkayyil, V. Kuttippurath, D.M. Chalil, N.R. Desai, C. Keloth, J. Phys. Chem. C **121**(48), 26976–26986 (2017)
111. Y. Fu, R.A. Ganeev, P.S. Krishnendu, C. Zhou, K.S. Rao, C. Guo, Opt. Mater. Express **9**(3), 976–991 (2019)
112. A. Haché, M. Bourgeois, Appl. Phys. Lett. **77**(25), 4089–4091 (2000)
113. S. Minissale, S.E.L.Ç.U.K. Yerci, L. Dal Negro, Appl. Phys. Lett. **100**(2), 021109 (2012)
114. S. Vijayalakshmi, F. Shen, H. Grebel, Appl. Phys. Lett. **71**(23), 3332–3334 (1997)
115. S.R. Flom, G. Beadie, S.S. Bayya, B. Shaw, J.M. Auxier, Appl. Opt. **54**(31), F123–F128 (2015)
116. S. Zhang, N. Dong, N. McEvoy, M. O'Brien, S. Winters, N.C. Berner, C. Yim, Y. Li, X. Zhang, Z. Chen, L. Zhang, ACS Nano **9**(7), 7142–7150 (2015)

117. S. Mirershadi, F. Sattari, A. Alipour, S.Z. Mortazavi, Front. Phys. **8**, 96 (2020)
118. Z. Liu, Y. Wang, X. Zhang, Y. Xu, Y. Chen, J. Tian, Appl. Phys. Lett. **94**(2), 021902 (2009)
119. Z. Zheng, C. Zhao, S. Lu, Y. Chen, Y. Li, H. Zhang, S. Wen, Opt. Express **20**(21), 23201–23214 (2012)
120. Y. Jiang, L. Miao, G. Jiang, Y. Chen, X. Qi, X.F. Jiang, H. Zhang, S. Wen, Sci. Rep. **5**(1), 1–12 (2015)
121. P.L. Li, Y.H. Wang, M. Shang, L.F. Wu, X.X. Yu, Carbon **159**, 1–8 (2020)
122. M.Z. Alam, I. De Leon, R.W. Boyd, Science **352**, 795–797 (2016)
123. O. Reshef, E. Giese, M.Z. Alam, I. De Leon, J. Upham, R.W. Boyd, Opt. Lett. **42**(16), 3225–3228 (2017)
124. H.I. Elim, W. Ji, F. Zhu, Appl. Phys. B **82**, 439–442 (2006)
125. D.F. Eaton, Science **253**(5017), 281–287 (1991)
126. W. Nie, Adv. Mater. **5**(7–8), 520–545 (1993)
127. B. Guo, Q.L. Xiao, S.H. Wang, H. Zhang, Laser Photonics Rev. **13**(12), 1800327 (2019)
128. J. Squier, M. Müller, Rev. Sci. Instrum. **72**(7), 2855–2867 (2001)
129. A. Bednarkiewicz, E.M. Chan, A. Kotulska, L. Marciniak, K. Prorok, Nanoscale Horiz. **4**(4), 881–889 (2019)
130. B. Liu, C. Chen, X. Di, J. Liao, S. Wen, Q.P. Su, X. Shan, Z.-Q. Xu, L.A. Ju, C. Mi, F. Wang, D. Jin, Nano Lett. **20**(7), 4775–4781 (2020)
131. M. Gu, H. Bao, X. Gan, N. Stokes, J. Wu, Light: Sci. Appl. **3**(1), e126–e126 (2014)
132. M.E. Maldonado, A. Das, A.S.L. Gomes, A.A. Popov, S.M. Klimentov, A.V. Kabashin, Opt. Lett. **45**, 6695–6698 (2020)
133. Y. Liu, F. Wang, H. Lu, G. Fang, S. Wen, C. Chen, X. Shan, X. Xu, L. Zhang, M. Stenzel, D. Jin, Small **10**(1002), 201905572 (2020)